A MAGNETIC FIELD MODEL FOR THE UNDULATOR IN HLS*

He Zhang#, Lin Wang, NSRL, USTC, Hefei, Anhui, P.R.China
Yongjun Li, DESY, Hamburg

Abstract

It is important to understand the influence of wigglers and undulators on the beam dynamics in design and optimization of a storage ring, especially when the storage ring runs on a low emittance mode. We present an analytic model of the undulator field in HLS, which can be used in the tracking study to evaluate the effects of it. Coefficients needed by the model are generated by fitting to the results of a numerical field caculation. Fringe fields are included in this model. Then we use three different methods to track particles through the undulator, and compare the results.

INTRODUCTION

Two insertion devices are installed in the HLS storage ring, a superconductive wiggler and a planar pure permanent-magnet undulator. They work well when the storage ring runs on the general purpose light source (GPLS) mode. The operation of an optical krystron is also on plan.

Now we are trying to find a low emittance mode lattice that is suitable to insertion devices. In this condition, the nonlinear components of the insertion devices magnetic field maybe one of the main limitations of the dynamic aperture[1]. So the tracking study of the particles through the insertion devices is necessary to get the transfer maps, which is a prerequisite for the study of particle dynamics of the whole ring. We use three methods, Runge-Kutta integration, symplectic integration, and generating function to do tracking and to construct transfer maps. An analytic field model is necessary or convenient to use these methods.

In this article, we build a field model of the undulator in the HLS storage ring, and get the transfer map of it. The similar methods can also be used to treat the wiggler and the optical krystron in HLS.

FIELD MODEL FOR THE UNDULATOR IN HLS

The undulaor (UD1) in HLS is designed to produce tunable, quasi-monochromatic, partially coherent radiation, the frequency of which is in the range from VUV to soft X-ray. Some parameters of the UD1 are given in Table 1.

The three-dimensional magnetic field data of UD1 versus position is calculated by RADIA[2]. To get the magnetic field model, we treat the periodic field and the fringe fields separately. The periodic field is described as the following form:

Table1: Parameters of the undulator in HLS

Magnet type	Permanent magnet
Period length	0.092 m
Period number	29
Range of the magnet gap	0.036 ~ 0.096 m
Peak field	0.456 ~ 0.06 T
Total length	2.67 m

$$\begin{aligned} B_x &= -\sum_i \frac{k_{xi}}{k_{yi}} B_i \sin(k_{xi}x)\sinh(k_{yi}y)\cos(k_i z) \\ B_y &= \sum_i B_i \cos(k_{xi}x)\cosh(k_{yi}y)\cos(k_i z) \\ B_z &= -\sum_i \frac{k_i}{k_{yi}} B_i \cos(k_{xi}x)\sinh(k_{yi}y)\sin(k_i z) \end{aligned} \quad (1)$$

where $k_{yi}^2 = k_{xi}^2 + k_i^2$, $k_i = i \cdot 2\pi / \lambda$ is the wave number of i^{th} harmonic along longitudinal direction, B_i is its peak magnetic field amplitude, $\lambda = 92$ mm is the period length of the undulator. These expressions of magnetic field satisfy Maxwell's equations.

By choosing the gauge $A_z = 0$, the corresponding vector potential $\boldsymbol{A} = (A_x, A_y, 0)$ is given by the following form:

$$\begin{aligned} A_x &= \sum_i \frac{1}{k_i} B_i \cos(k_{xi}x)\cosh(k_{yi}y)\sin(k_i z) \\ A_y &= \sum_i \frac{k_{xi}}{k_{yi}k_i} \sin(k_{xi}x)\sinh(k_{yi}y)\sin(k_i z) \end{aligned} \quad (2)$$

Because of the symmetry of the periodic magnetic field, only the odd harmonics are used to fit the magnetic data. Given a calculation of the field at a set of points, the problem is to find a sum of terms, which minimize the variance between field calculation data and fit data. The fit results are listed in Table 2. Field calculation results and fit curves of B_y as a function of x, y and z are shown in Figure 1. Only 3 terms are used for the fit. The peak field is about 0.41 T and the RMS difference between calculation data and fit data is 8.5 Gauss, which gives an RMS to peak field ratio of 0.17%.

Table2: Fit results of the periodic field

i	B_i (T)	k_{xi} (/mm)	k_{yi} (/mm)	k_i (/mm)
1	-4.1299e-1	-1.1425e-2	6.9244e-2	6.8295e-2
3	2.7615e-5	6.7879e-2	2.1584e-1	2.0489e-1
5	7.6398e-4	5.0851e-3	3.4152e-1	3.4148e-1

*Work supported by CAS Knowledge Innovation Project
#zhanghe@ustc.edu

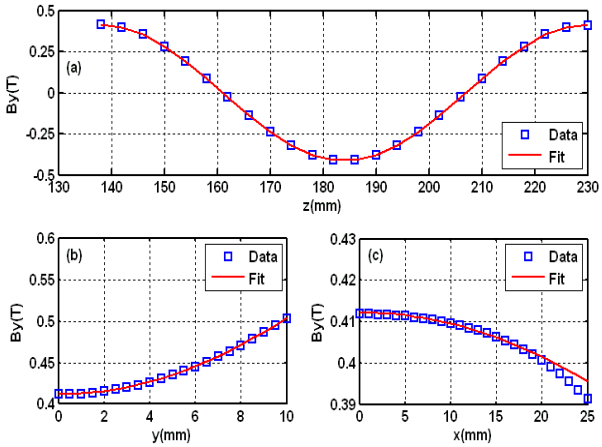

Figure 1: (a) B_y as a function of z at $x = y = 0$. (b) B_y as a function of y at $x = 0$, $z = 138$mm. (c) B_y as a function of x at $y = 0$, $z = 138$mm.

The fringe fields are described as the following form:

$$B_x = -\sum_i \frac{k_{xi}}{k_{yi}} \sin(k_{xi}x)\sinh(k_{yi}y)B_i(z)$$

$$B_y = \sum_i \cos(k_{xi}x)\cosh(k_{yi}y)B_i(z) \qquad (3)$$

$$B_z = -\sum_i \frac{k_i}{k_{yi}} \cos(k_{xi}x)\sinh(k_{yi}y)B_i(z)$$

$$with \quad B_i(z) = B_{1i}\cos k_i z + B_{2i}\sin k_i z$$

where $k_{yi}^2 = k_{xi}^2 + k_i^2$, k_i and B_i have the same meaning as in equation (1) except that $\lambda = 300$ mm here. These expressions also satisfy Maxwell's equations.

By choosing the gauge $A_z = 0$, the corresponding vector potential $\boldsymbol{A} = (A_x, A_y, 0)$ is given by the following form:

$$A_x = \sum_i \frac{1}{k_i} \cos(k_{xi}x)\cosh(k_{yi}y)A_i(z)$$

$$A_y = \sum_i \frac{k_{xi}}{k_{yi}k_i} \sin(k_{xi}x)\sinh(k_{yi}y)A_i(z) \qquad (4)$$

$$with \quad A_i(z) = B_{1i}\sin(k_i z) - B_{2i}\cos(k_i z)$$

We use the similar method with what we use in the periodic field case to fit fringe fields. But in the case of fringe fields, both the odd and the even harmonics must be used to fit the data, and more terms are needed. In fact, we used 20 terms to make sure that the RMS difference between calculation data and fit data is 5.7 Gauss which gives an RMS to peak field ratio of 0.11%. Figure 2 shows field calculation results and fit curves of B_y as a function of x, y and z.

Since the field model has already been calculated, the Hamiltonian of charged particle motion in either period field or fringe fields in the paraxial approximation can be written as[3]:

$$H(z) = \frac{(p_x - a_x)^2}{2(1+\delta)} + \frac{(p_y - a_y)^2}{2(1+\delta)} - a_z \qquad (5)$$

where $p_{x,y} = P_{x,y}/P_0$ is the scaled transverse momenta, P_0 is the nominal mechanical momentum, $\boldsymbol{a} = q\boldsymbol{A}/P_0 c$ is the scaled vector potential, $\delta = \Delta E / P_0 c$ is the relative energy deviation.

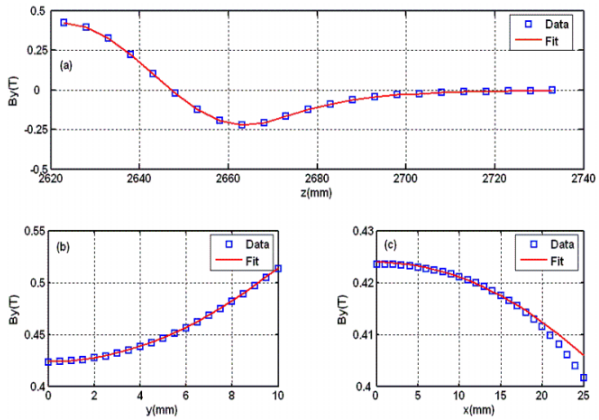

Figure 2: (a) B_y as a function of z at $x = y = 0$. (b) B_y as a function of y at $x = 0$, $z = 2623$mm. (c) B_y as a function of x at $y = 0$, $z = 2623$mm.

TRACKING METHODS AND RESULTS

After getting an analytic model of the undulator field, we use three methods to track particles through the undulator.

The first one is solving the equations of motion with a Runge-Kunge type integration (RK). This method is not symplectic. And when the undulator has many periods, this method is rather slow. But because it is derived directly from the equations of motion, it can be used to verify other methods.

The second method is symplectic integration (SI)[4]. This method requires splitting each period of field into enough pieces, so it is also time consuming, especially for a long undulator or wiggler.

The third method is building a generating function (GF)[5]. The generating function has a form :

$$F(x_i, x'_f, y_i, y'_f) = \sum_{k+l+m+n}^{4} x_i^{\,k} x'^{\,l}_f y_i^{\,m} y'^{\,n}_f \qquad (6)$$

where subscript i and j represent the initial and final state of particles passing through the undulator. Coefficients are generated by fitting to the tracking results of numerous particles with different initial states. This procedure is also time consuming, but it is needed only once. Tracking through the generating function is fast and symplectic.

Figure 3 and Figure 4 show the tracking simulation results of the three methods. Figure 3 (a) shows the tracking results of x'_f as a function of x_i. The result of SI and the result of GF agree well, better than 0.001mrad. The difference between RK and them is less than 0.01mrad. Figure 3 (b) shows y'_f as a function of x_i. The results of SI and RK agree better than 0.002mrad, while the difference between GF and them is less than 0.012mrad.

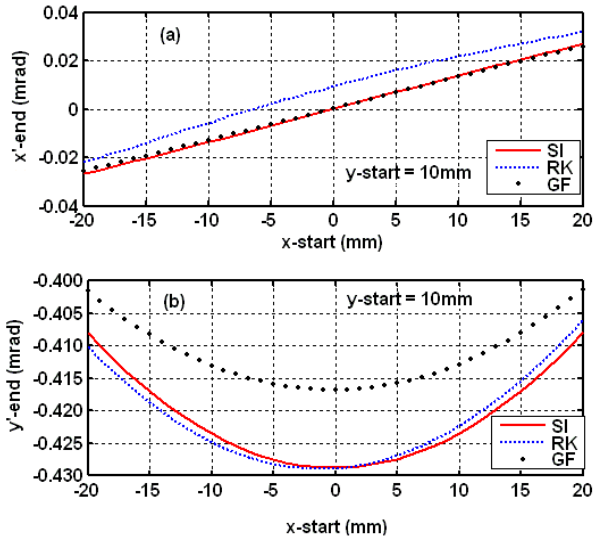

Figure 3: (a) x'_f as a function of x_i using three different tracking methods in the case $x'_i = y'_i = 0$ and y_i = 10mm. (b) y'_f as a function of x_i.

Figure 4 (a) shows the tracking results of x'_f as a function of y_i. The results of GF and SI agree better than 0.001mrad, and the difference between RK and them is less than 0.011mrad. Figure 4 (b) shows y'_f as a function of y_i, and Figure 4 (c) shows the difference of y'_f using the three methods as the function of y_i. As it shows, the further y_i leaves the axis, the larger the difference is. But the largest difference between SI and RK is less than 0.002mrad, difference between GF and RK less than 0.005mrad, and difference between SI and GF less than 0.007mrad.

If we only track particles through the periodic field, the tracking results of x'_f using the three methods agree better than 0.001mrad. So the difference showed in Figure 3 (a) and Figure 4 (a) attributes to the existence of fringe fields. The reason why the tracking results of RK and SI do not agree well in the fringe fields needs more particular analysis later. The difference between GF and the other two methods showed in Figure 3 (b) is also reasonable. In the fitting data used to calculate the generating function coefficients, the maximum of y_i is only 0.2mm. So it is natural that GF is no longer accurate when y_i is much larger than 0.2mm, 10mm in this case. This fact is also consistent with Figure 4 (c), and it suggests that choosing proper data to fit the generating function coefficients is necessary. But why does GF agree well with SI and RK as Figure 4 shows, when x_i = 20mm, which is much larger than 0.2mm, the maximum of the fit data x_i? In Figure 1 and Figure 2, we can see that when y_i changes 10 mm, B_y changes 0.1T. Correspondingly when x_i changes 20mm, B_y changes only a little more than 0.01T. So the change of x_i affects much little than the change of y_i.

CONCLUSIONS

The accurate undulator field model including fringe fields represented here makes possible the symplectic mapping which is necessary in long term tracking. In the three tracking methods, GF is chosen for later tracking simulation because of its speed and symplecticity. Similar methods can be used to treat the wiggler and the optical krystron in HLS, generating their models, building their generating functions, and thereby evaluating their dynamical effects by tracking simulation.

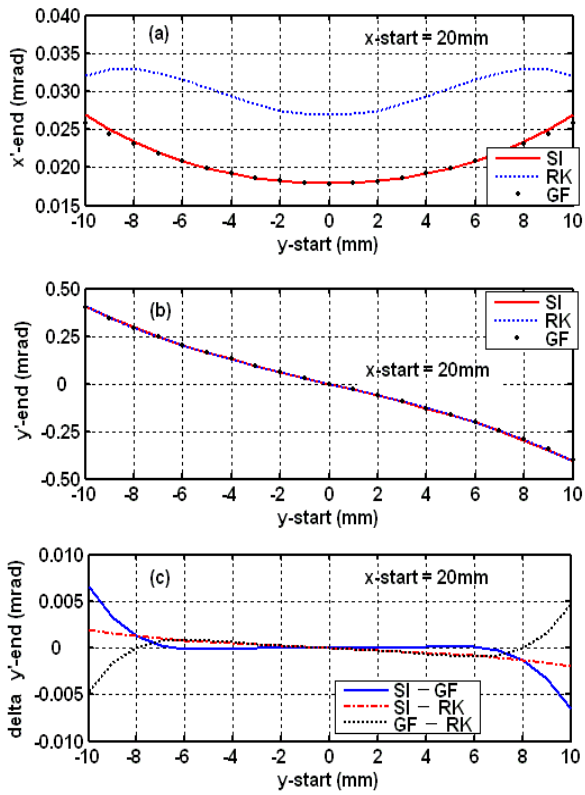

Figure 4: (a) x'_f as a function of y_i using three tracking methods in the case $x_i = y_i = 0$ and x_i = 20mm. (b) y'_f as a function of y_i. (c) Difference of y'_f between either two of the three tracking methods as a function of y_i.

REFERENCES

[1] L. Smith, "Effects of Wigglers and Undulators on Beam Dynamics", LBL-ESG, Tech, Note-24, 1986.

[2] A Three-Dimensional Magnetostatic Computer Code, http://www.esrf.fr/Accelerators/Groups/InsertionDevices/Software/Radia.

[3] Y. K. Wu, etc, "Explicit Symplectic integrator for s-dependent static magnetic field." Phys. Review E 68(2003), 046502.

[4] Y. Li, etc, "Study of Insertion Device's on Nonlinear Beam Dynamics in Electron Storage Ring Using Lie Algebra", HEP&NP, 2003, 27(9), (in Chinese).

[5] K. Balewski, etc, "Beam Dynamics Study For PETRA III Including Damping Wigglers", EPAC'04, p. 1999.